

# Spin-orbit interaction and spin coherence in narrow-gap semiconductor and semimetal wires

J. J. Heremans,<sup>a</sup> R. L. Kallaher,<sup>a</sup> M. Rudolph,<sup>a</sup> M. B. Santos,<sup>b</sup> W. Van Roy,<sup>c</sup> G. Borghs<sup>c</sup>

<sup>a</sup>Department of Physics, Virginia Tech, Blacksburg, VA 24061, USA

<sup>b</sup>Homer L. Dodge Department of Physics and Astronomy, University of Oklahoma, Norman, OK 73019, USA

<sup>c</sup>IMEC, Kapeldreef 75, B-3001, Leuven, Belgium

**Abstract.** Spin-dependent quantum transport experiments on InSb and InAs heterostructures and Bi thin films are discussed, focusing on mesoscopic geometries where spin-orbit interaction and quantum coherence determine the properties. The narrow-bandgap semiconductors InSb and InAs, and the semimetal Bi have substantial spin-orbit interaction. The experiments use antilocalization to study spin-orbit interaction and spin coherence lengths in nanolithographic wires fabricated on the materials. In the three systems the spin coherence lengths increase with decreasing wire widths if other parameters stay constant, of technological importance for spin-based devices. The experiments also indicate that Bi has surface states with Rashba-like spin-orbit interaction. A quasi-one-dimensional model of antilocalization, as fitted to the data, is explained and its consequences for quantum coherence in mesoscopic structures is explored. A unified understanding of the experiments is presented relying on the duality between the Aharonov-Bohm and the Aharonov-Casher phases, the latter resulting from spin-orbit interaction. The duality strengthens the analogy between phenomena under magnetic fields and under spin-orbit interaction.

**Keywords:** spin-orbit interaction, spin coherence, InSb, InAs, bismuth, mesoscopic.

**Address all correspondence to:** Jean J. Heremans, Virginia Polytechnic Institute and State University, Department of Physics, 850 West Campus Drive, Blacksburg, VA 24061, Tel: 1 540-231-4604; E-mail: [heremans@vt.edu](mailto:heremans@vt.edu)

## 1 Introduction

Wires of materials with strong spin-orbit interaction (SOI) are of current interest as hosts for quantum states with non-Abelian Majorana properties under proximity-induced superconductivity.<sup>1,2</sup> Strong spin-orbit interaction also inspires avenues for constructing new quantum states of matter, in analogy to quantum states at high magnetic fields. Materials with strong SOI include the narrow-bandgap semiconductors InSb and InAs, and the semimetal bismuth. In this context, the present work experimentally studies spin-related quantum transport phenomena in systems with strong SOI at mesoscopic scales, namely InSb, InAs and Bi submicron wires lithographically fabricated from epitaxial materials. At reduced dimensions, the wire width and length interact with the spin coherence length or spin precession length, the quantum phase coherence length, and the elastic mean-free-path to modify the quantum transport signatures, as measured by antilocalization (AL). The AL quantum correction to the magnetoresistance results from electron interference on time-reversed trajectories, and as a quantum interference experiment is sensitive to spin coherence lengths.<sup>3-6</sup> In InSb quantum wells, InAs quantum wells, and Bi thin films, our experiments<sup>7-9</sup> show the spin coherence lengths  $L_{so}$  increasing with decreasing wire widths  $w$  if other parameters stay constant. Several other experimental investigations of spin coherence in wires with SOI exist,<sup>10-14</sup> as well as theoretical work.<sup>3</sup> These investigations likewise indicate that  $L_{so}$  increases as  $w$  is reduced. This observation has technological importance for nanoscaled spintronics. Yet more fundamentally, we will show that a unified understanding of the results appears via the duality between the Aharonov-Bohm<sup>15</sup> phase under magnetic fields  $B$  and the Aharonov-Casher<sup>16-18</sup> phase

under SOI, underscoring the analogy between the physics of solid-state systems under magnetic fields and under SOI. The experiments are also consistent with Bi having surface states with strong Rashba-like SOI.<sup>9,19–21</sup>

The magnetotransport measurements are performed through sets of wires using 4-terminal low-frequency lock-in techniques at low temperatures  $T \approx 0.39$  K and at low  $B$  applied perpendicularly to the plane of the samples. The data is analyzed in quasi-one-dimensional (Q1D) AL theory to obtain the dependence on  $w$  of  $L_{so}$ . The wires are in the Q1D regime, where  $w$  is comparable to or shorter than  $L_{so}$ , than the quantum phase coherence length  $L_\phi$  and than the elastic mean-free-path  $l_e$ . The quantitative predictions afforded by AL theory<sup>5,6,22</sup> for the dependence of the conductance  $G$  on  $L_{so}$  and  $L_\phi$  as function of  $B$  allows values for  $L_{so}$  and  $L_\phi$  to be obtained from a fit of the experimental  $G(B)$  to theory. The present work uses an AL approach adapted specifically to Q1D wires.<sup>7,8</sup>

## 2 Experimental aspects

The  $\text{In}_{0.85}\text{Al}_{0.15}\text{Sb}/\text{InSb}/\text{In}_{0.85}\text{Al}_{0.15}\text{Sb}$  (InSb quantum well thickness 25 nm, properties described in Ref. 7) and  $\text{Al}_{0.3}\text{Ga}_{0.7}\text{Sb}/\text{InAs}/\text{Al}_{0.3}\text{Ga}_{0.7}\text{Sb}$  (InAs quantum well thickness 15 nm, properties described in Ref. 8) heterostructures are grown by molecular beam epitaxy on (001) GaAs substrates. At 0.39 K the unpatterned InSb quantum well shows an areal carrier density  $5.2 \times 10^{15} \text{ m}^{-2}$  with mobility  $9.7 \text{ m}^2/\text{Vs}$  ( $l_e \approx 3.3 \mu\text{m}$ ), and the InAs quantum well  $9.9 \times 10^{15} \text{ m}^{-2}$  with mobility  $15 \text{ m}^2/\text{Vs}$  ( $l_e \approx 6.4 \mu\text{m}$ ). Necessary parameters for the quantum wells are calculated assuming non-parabolicity. On both materials, wires of length  $L=24 \mu\text{m}$  are fabricated using electron-beam lithography and reactive ion etching, with wire sets of different  $w$  integrated on the same chip to ensure uniform properties. Bi(111) thin films are obtained by thermally evaporating Bi (99.999%) onto a  $\text{SiO}_2$  (oxidized Si(001)) substrate,<sup>9</sup> in 2-step deposition for films with the largest grain sizes and fewest defects.<sup>23</sup> X-ray diffraction reveals films oriented with their trigonal axis perpendicular to the substrate, typical for this growth method,<sup>24</sup> with grains of size 200-500 nm randomly oriented. The trigonal face (Bi(111) in rhombohedral, Bi(001) in short hexagonal notation) is thus exposed. The total film thickness as optimized for quantum transport measurements is 75 nm.<sup>23</sup> Multicarrier fits to the longitudinal and transverse magnetoresistances indicate compensated electron and hole densities as expected for high-quality Bi. Electron and hole densities are  $\sim 2 \times 10^{24} \text{ m}^{-3}$  and mobilities  $\sim 0.1 \text{ m}^2/\text{Vs}$ . The AL measurements however appear dominated by surface carriers, predicted to exist on Bi(111).<sup>19–21</sup> The surface Fermi surface of Bi(111) consists of a central electron pocket (along the trigonal axis) and six hole ellipses along the binary axes, and our results can be interpreted as resulting from the electron pocket (effective mass  $\sim 0.5 m_e$  with  $m_e$  the free electron mass). On Bi, wires with  $L=16 \mu\text{m}$  are fabricated using electron-beam lithography and wet etching. In all three materials, effects of transverse quantization are neglected, because the Fermi wavelengths indicate that many (10 to 40) transverse subbands are populated.

As an example, Fig. 1 shows the measured change in resistance  $R = 1/G$ , as  $\Delta R/R^2$  where  $\Delta R = R(B) - R(0)$ , in Bi wires ( $w$  as indicated) at  $T = 0.39$  K as function of applied  $B$  (noting that  $\Delta R/R^2 \approx -\Delta G$ ). The data display the characteristic shape of antilocalization:  $\Delta R$  increases sharply as  $|B|$  is initially increased from zero. Mesoscopic universal conductance fluctuations<sup>9</sup> are also present in the wires. Below we describe the model fitted to this data and equivalent data on InSb and InAs wires, from which values of  $L_{so}$  can be extracted.

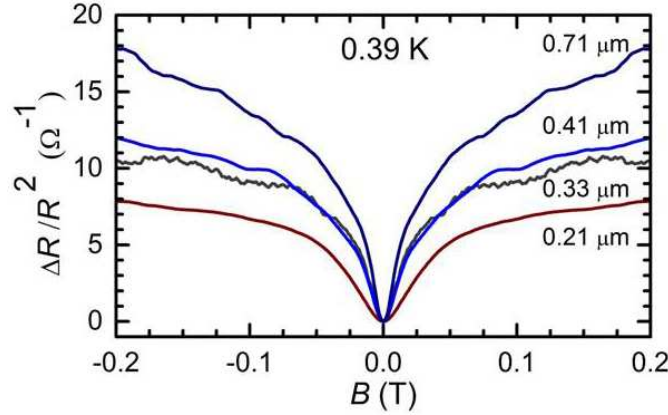


**Fig 1** Magnetoconductance due to AL measured in Bi wires of widths 0.21, 0.33, 0.41 and 0.71  $\mu\text{m}$ .

### 3 Q1D approach to antilocalization

The quantum correction to the 2-dimensional (2D) conductivity  $\sigma_{2D} = (L/w)G$  depends on the length over which a wave packet retains coherence and in a system of width  $w$  at  $B = 0$  and without SOI can be expressed as<sup>25,26</sup> (per spin channel):

$$\delta\sigma_{2D} = -\frac{1}{2} \frac{e^2}{\pi\hbar} \frac{L_\phi}{w} \quad (1)$$

Under applied  $B$ ,  $L_\phi$  is reduced by time-reversal symmetry breaking to an effective coherence length, limited by a magnetic length  $L_B$ .<sup>3,25,27</sup> Under SOI,  $L_\phi$  is further replaced by a combination of singlet and triplet<sup>3,5,7,8,25,28,29</sup> length scales originating in pairing of time-reversed trajectories (Cooperons). The singlet  $L_{0,0}$  and triplet  $L_{1,m}$  ( $m = \pm 1, 0$ ) length scales are:

$$\begin{aligned} L_{0,0} &= (L_\phi^{-2} + L_B^{-2})^{-\frac{1}{2}} \\ L_{1,\pm 1} &= (L_\phi^{-2} + L_{so}^{-2} + L_B^{-2})^{-\frac{1}{2}} \\ L_{1,0} &= (L_\phi^{-2} + 2L_{so}^{-2} + L_B^{-2})^{-\frac{1}{2}} \end{aligned} \quad (2)$$

The singlet  $L_{0,0}$  is not sensitive to spin decoherence under SOI.<sup>7,8,29</sup> The difference between  $L_{1,\pm 1}$  and  $L_{1,0}$  arises from anisotropic spin decoherence in 2D systems,<sup>6</sup> and disappears in 3D systems.<sup>25,28</sup> In unconstrained (wide) 2D systems,  $L_B = l_m \equiv \sqrt{\hbar/eB}$ . When the 2D system is narrowed to a Q1D wire with  $w \lesssim l_m$  and  $w \lesssim l_e$ , the wave function boundary conditions and ballistic flux cancellation (respectively) have to be considered, and, for low  $B$ ,  $L_B$  is modified to:<sup>7,8,27,30</sup>

$$L_B = l_m \sqrt{\left( \frac{C_1 l_m^2 l_e}{w^3} \right)} \quad (3)$$

Here  $C_1 = 4.75$  for specular boundary scattering and  $C_1 = 2\pi$  for diffusive boundary scattering.<sup>7,8,27</sup> Equation (3) assumes  $l_e \gtrsim 0.6w$ . The effect of  $L_B$  is to delay flux accumulation to higher  $B$  in a narrow wire, and hence to spread out the magnetoconductance features over higher  $B$ . The

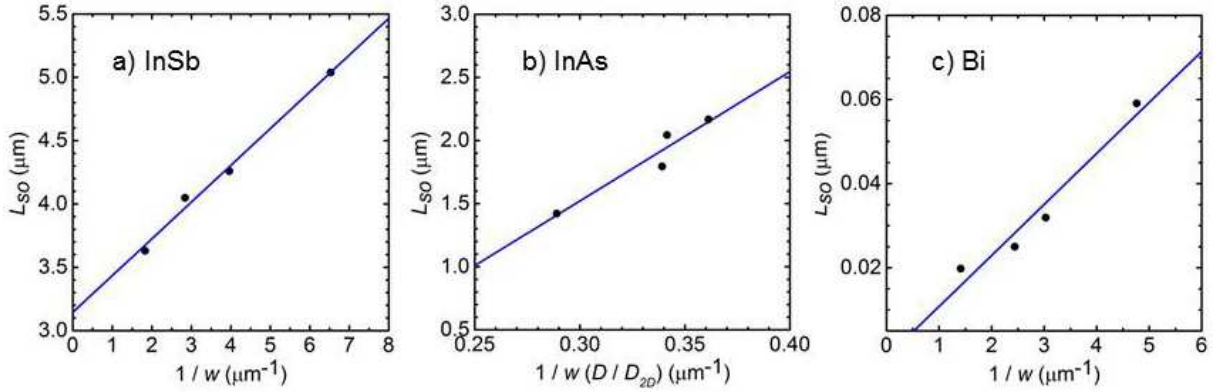


**Fig 2** Experimental values of  $L_{so}$  vs  $1/w$  for wires of width  $w$  fabricated on (a) an InSb 2D system, (b) an InAs 2D system, and (c) a Bi thin film.

quantum correction  $\delta\sigma_{2D}$  is related to the measured conductance correction  $\delta G(B) = G(B) - G_0$ , by  $\delta G(B) = (w/L)\delta\sigma_{2D}$ , with  $G_0$  the classical conductance of the wire. The  $B$  dependence of  $\delta G(B)$  reduces to a combination of length ratios:<sup>7,8,25,28</sup>

$$\delta G(B) = -\frac{1}{2} \frac{e^2}{\pi \hbar} \frac{1}{L} (L_{1,1}f(L_{1,1}) + L_{1,-1}f(L_{1,-1}) + L_{1,0}f(L_{1,0}) - L_{0,0}f(L_{0,0})) \quad (4)$$

The experimental data can be compared to fits to Eq. (4) because  $\Delta G = G(B) - G(0) = \delta G(B) - \delta G(0)$ . The function  $f(L_{s,m})$  enters due to modifications to quantum interference in coherent mesoscopic geometries. In unconstrained 2D systems or wires with  $L \rightarrow \infty$  or  $L \gtrsim 10 L_{s,m}$  we have  $f = 1$ . In a wire of finite  $L$ , interactions with the wide regions at both ends of the wire reduce coherence to yield:<sup>7,31</sup>

$$f(L_{s,m}) = \coth\left(\frac{L}{L_{s,m}}\right) - \frac{L_{s,m}}{L}. \quad (5)$$

Values for  $L_{so}$  are found by fitting  $\Delta G$  to Eq. (4), with Eqs. (2), (3), (5), which together capture the experiments well. Experimental values for  $L_{so}$  vs  $1/w$  for InSb and InAs quantum wells, and Bi thin films are presented in Fig. 2. Our experiments<sup>7-9</sup> show  $L_{so} \propto 1/w$  if other parameters stay constant (in InAs wires the diffusion constant  $D$  is reduced compared to the 2D value  $D_{2D}$  as  $w$  narrows; this is accounted for in Fig. 1, as explained in Ref. 8). Prior to discussing the results, we explore geometrical consequences for AL implied by Eqs. (2)- (5). Figure 3 shows results from Eqs. (2)- (5) using approximate InSb wire experimental parameters<sup>7</sup> at  $T = 0.39$  K ( $l_e = 3.3 \mu\text{m}$ ,  $L_\phi = 15 \mu\text{m}$ ) plotted as  $\Delta R/R^2 \approx -\Delta G = -(\delta G(B) - \delta G(0))$ . The effect of  $w$  is depicted in Fig. 3a, where we assumed values for  $w$  (top to bottom curves:  $0.56, 0.36, 0.26, 0.16 \mu\text{m}$ ) and for  $L_{so}$  (respectively  $3.6, 4.0, 4.3, 5.0 \mu\text{m}$ ) at fixed  $L = 24 \mu\text{m}$  as in Fig. 2a. The lengthening of  $L_{so}$  with narrowing  $w$  implies a reduction in the SOI strength, and would imply a decrease in separation in  $B$  between maxima of  $\Delta R/R^2$ . However, at narrow  $w$  the delay to higher  $B$  of flux accumulation (Eq. (3)) counteracts the effect of decreasing SOI and spreads the maxima to higher  $B$ . The decreasing SOI with narrowing  $w$  is then mostly seen in the decreased depth of the AL dip in  $\Delta R/R^2$  around  $B \sim 0$ . The effect of  $L$  is depicted in Fig. 3b, where we assumed (top

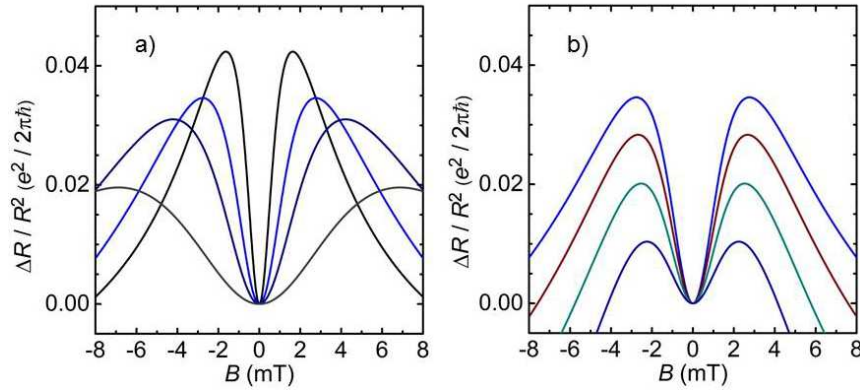


**Fig 3** Geometrical effects in wires of (a)  $w$ , and (b)  $L$ , on the AL signal  $\Delta R/R^2$ . In (a),  $w$  is varied (wide  $w$  at top, narrow  $w$  at bottom) and in (b)  $L$  is varied (long  $L$  at top, short  $L$  at bottom) as described in the text.

to bottom curves)  $L = 24, 21, 18$  and  $15 \mu\text{m}$ , at fixed  $w = 0.36 \mu\text{m}$  and  $L_{so} = 4.0 \mu\text{m}$ . Shortening  $L$  affects the depth of the AL dip in  $\Delta R/R^2$ , but does not appreciably shift the maxima since the effective  $L_B$  and  $L_{so}$  are unaffected. The reduction in AL signal with shortening  $L$  originates in Eq. (5), effectively shortening  $L_\phi$  (long in the unconstrained InSb system and hence susceptible to effects of  $f(L_{s,m})$ ). The effect of  $L$  via  $f(L_{s,m})$  illustrates the sensitivity of quantum coherence in mesoscopic structures to interactions with wide neighboring regions. Figure 3 illustrates that geometrical factors substantially impact AL signals.

#### 4 Discussion

Theoretical work<sup>3</sup> suggests that  $L_{so} \propto 1/w$  can be understood in terms of the effective vector potential due to SOI. In disordered wires ( $l_e < w$ ) with Rashba SOI<sup>32</sup> and under the D'yakanov-Perel (DP) motional narrowing spin decoherence mechanism, it is predicted<sup>3</sup> that  $L_{so} = \sqrt{12}L_\Omega^2/w$ , where the spin precession length  $L_\Omega = v_F/\Omega$  with  $\Omega$  the spin precession frequency under SOI, and  $v_F$  the Fermi velocity. The zero- $B$  spin-splitting energy for Rashba SOI is  $\hbar\Omega = 2k_F\alpha$  with  $k_F$  the Fermi wavevector and  $\alpha$  the Rashba SOI parameter. Under a parabolic dispersion with effective mass  $m^*$  we obtain  $L_\Omega = \hbar^2/(2m^*\alpha)$ .<sup>3,33</sup> The dependence  $L_{so} = \sqrt{12}L_\Omega^2/w$  is in contrast to unconstrained 2D systems, where  $L_{so} = L_\Omega$  under DP spin decoherence. The unconstrained spin decoherence rate then follows  $1/\tau_{so} = \Omega^2\tau_e/2$ , with  $\tau_e$  the momentum scattering time ( $l_e = v_F\tau_e$ ),<sup>3,6,10,33</sup> such that  $L_{so} = \sqrt{D\tau_{so}} = L_\Omega$ . Yet,  $L_{so} = \sqrt{12}L_\Omega^2/w$  in wires finds an analogy to  $L_B$  in wires,<sup>25,27</sup> where in the disordered case  $L_B = \sqrt{3}l_m^2/w$ , resulting from modifying the Landau basis for wave functions constrained to a wire (Eq. (3) is a ballistic adaptation), whereas in unconstrained systems,  $L_B = l_m$ . Hence, under SOI  $L_\Omega$  assumes the role of the magnetic  $l_m$ . Both  $L_{so}$  and  $L_B$  function to limit  $L_\phi$  in Eqs. (2) and thus limit quantum coherence effects in Eq. (4).

Insight in the relation  $L_B = \sqrt{3}l_m^2/w$  can be obtained by considering the effect of the Aharonov-Bohm<sup>15</sup> (AB) phase on quantum interference. A closed path of average radius  $l_m/\sqrt{\pi}$  encloses a magnetic flux  $\hbar/e$  and a particle over such path will accumulate a unity quantum phase. If the path is constrained to  $w$  along one direction, acquiring the same phase will require the particle traveling  $l_m^2/w$  in the orthogonal direction, which becomes the effective free length over which

the phase is affected. The relation  $L_B \propto l_m^2/w$  hence receives a geometrical interpretation. SOI can in the present case be mapped on the physics arising from an effective vector potential,<sup>34</sup> here  $\vec{A}_{ac} = (1/c^{*2})\vec{\mu} \times \vec{E}$ , where  $\vec{\mu}$  is the particle's magnetic moment,  $\vec{E}$  the actual or effective electric field breaking inversion symmetry and thereby giving rise to SOI, and  $c^*$  the effective velocity of light (a bandstructure parameter, akin to Ref. 35). We call  $\vec{A}_{ac}$  the Aharonov-Casher (AC) vector potential, as it enters in the AC phase<sup>16-18</sup> in the same way that the magnetic vector potential  $e\vec{A}$  enters in the AB phase. Using  $|\vec{\mu}| = \frac{1}{2}\mu_B$  with  $\mu_B$  the Bohr magneton,  $\vec{A}_{ac}$  maps to Rashba SOI,<sup>34</sup> with  $\alpha = |\vec{E}|(\hbar^2 e)/(4m^{*2}c^{*2})$ . Given the relation between  $l_m$  and the AB phase, we can now ask which characteristic AC length  $l_{ac}$  has a role equivalent to  $l_m$ . For Rashba SOI, we find  $l_{ac} = \hbar^2/(2m^*\alpha) = L_\Omega$ . We thus recover the observation that under SOI  $L_\Omega$  assumes the role of the magnetic  $l_m$ . The geometrical interpretation leading to  $L_B \propto l_m^2/w$  hence also leads to  $L_{so} \propto L_\Omega^2/w$ . The prefactors of order unity (insofar as they are borne out by experiments) require a more exact use of appropriate boundary conditions.

We note that AL measures  $L_{so}$  and experimental uncertainty may reside in the identity  $L_{so} = L_\Omega$ , valid only under DP spin decoherence. The experiments (Fig. 2) however suggest that indeed  $L_{so} \propto 1/w$ , and extracted values for  $L_\Omega$  are consistent with known SOI strengths.<sup>7,8</sup> Figure 2c indicates that measurements on Bi follow  $L_{so} \propto 1/w$ . The above arguments hold for 2D systems, and our quantum transport experiments hence suggest that Bi harbors surface states with Rashba-like SOI,<sup>19,21</sup> as ARPES measurements have indicated,<sup>20</sup> and that these surface states play an important role in the transport properties. The values for  $L_{so}$  for Bi are shorter than for InSb and InAs, indicating higher  $\alpha$  and stronger SOI than for the narrow-gap semiconductors, in accordance again with the literature.<sup>19-21</sup>

## 5 Conclusions

Antilocalization measurements allow the determination of the low-temperature spin coherence lengths in mesoscopic wires of InSb, InAs and Bi. In nanolithographic wires of all three materials, it is observed that the spin coherence lengths increase proportionally to the inverse wire widths. This observation is compatible with theoretical arguments using an effective spin-orbit vector potential leading to a modification of the wave functions boundary conditions in a narrow wire. A quasi-one-dimensional approach to antilocalization is further used to demonstrate geometric effects of confinement on quantum coherence in mesoscopic wires.

### Acknowledgments

The work was supported by the U.S. Department of Energy, Office of Basic Energy Sciences, Division of Materials Sciences and Engineering under award DOE DE-FG02-08ER46532 (JJH), and by the National Science Foundation under award DMR-0520550 (MBS).

### References

- 1 V. Mourik, K. Zuo, S. M. Frolov, S. R. Plissard, E. P. A. M. Bakkers, and L. P. Kouwenhoven, "Signatures of Majorana Fermions in hybrid superconductor-semiconductor nanowire devices," *Science* **336**, 1003–1007 (2012).

- 2 L. P. Rokhinson, X. Liu, and J. K. Furdyna, "The fractional a.c. Josephson effect in a semiconductor-superconductor nanowire as a signature of Majorana particles," *Nature Phys.* **8**, 795–799 (2012).
- 3 S. Kettemann, "Dimensional control of antilocalization and spin relaxation in quantum wires," *Phys. Rev. Lett.* **98**, 176808 (1–4) (2007).
- 4 G. Bergmann, "Weak-localization in thin films, a time-of-flight experiment with conduction electrons," *Phys. Rep.* **107**, 1–58 (1984).
- 5 S. Hikami, A. I. Larkin, and Y. Nagaoka, "Spin-orbit interaction and magnetoresistance in the two dimensional random systems," *Prog. Theor. Phys.* **63**, 707–710 (1980).
- 6 S. V. Iordanskii, Y. B. Lyanda-Geller, and G. E. Pikus, "Weak localization in quantum wells with spin-orbit interaction," *JETP Lett.* **60**, 206–211 (1994).
- 7 R. L. Kallaher, J. J. Heremans, N. Goel, S. J. Chung, and M. B. Santos, "Spin and phase coherence lengths in n-InSb quasi-one-dimensional wires," *Phys. Rev. B* **81**, 035335 (1–7) (2010).
- 8 R. L. Kallaher, J. J. Heremans, W. V. Roy, and G. Borghs, "Spin and phase coherence lengths in InAs wires with diffusive boundary scattering," *Phys. Rev. B* **88**, 205407 (1–7) (2013).
- 9 M. Rudolph and J. J. Heremans, "Spin-orbit interaction and phase coherence in lithographically defined bismuth wires," *Phys. Rev. B* **83**, 205410 (1–6) (2011).
- 10 A. W. Holleitner, V. Sih, R. C. Myers, A. C. Gossard, and D. D. Awschalom, "Suppression of spin relaxation in submicron InGaAs wires," *Phys. Rev. Lett.* **97**, 036805 (1–4) (2006).
- 11 T. Schaepers, V. A. Guzenko, M. G. Pala, U. Zuelicke, M. Governale, J. Knobbe, and H. Hardtdegen, "Suppression of weak antilocalization in GaInAs/InP narrow quantum wires," *Phys. Rev. B* **74**, 081301(R) (1–4) (2006).
- 12 Y. Kunihashi, M. Kohda, and J. Nitta, "Enhancement of spin lifetime in gate-fitted InGaAs narrow wires," *Phys. Rev. Lett.* **102**, 226601 (1–4) (2009).
- 13 D. Liang, J. Du, and X. Gao, "Anisotropic magnetoconductance of a InAs nanowire: angle-dependent suppression of one-dimensional weak localization," *Phys. Rev. B* **81**, 153304 (1–4) (2010).
- 14 P. Roulleau, T. Choi, S. Riedi, T. Heinzl, I. Shorubalko, T. Ihn, and K. Ensslin, "Suppression of weak antilocalization in InAs nanowires," *Phys. Rev. B* **81**, 155449 (1–4) (2010).
- 15 Y. Aharonov and D. Bohm, "Significance of electromagnetic potentials in quantum theory," *Phys. Rev.* **115**, 485–491 (1959).
- 16 Y. Aharonov and A. Casher, "Topological quantum effects for neutral particles," *Phys. Rev. Lett.* **53**, 319–321 (1984).
- 17 J. Anandan, "Classical and quantum interaction of the dipole," *Phys. Rev. Lett.* **85**, 1354–1357 (2000).
- 18 L. L. Xu, S. Ren, and J. J. Heremans, "Magnetoelectronics at edges in semiconductor structures: helical Aharonov-Casher edge states," *Integr. Ferroelectr.* **131**, 36–46 (2011).
- 19 P. Hofmann, "The surfaces of bismuth: Structural and electronic properties," *Prog. Surf. Sci.* **81**, 191–245 (2006).

- 20 T. Hirahara, K. Miyamoto, I. Matsuda, T. Kadono, A. Kimura, T. Nagao, G. Bihlmayer, E. V. Chulkov, S. Qiao, K. Shimada, H. Namatane, M. Taniguchi, and S. Hasegawa, "Direct observation of spin splitting in bismuth surface states," *Phys. Rev. B* **76**, 153305 (1–4) (2007).
- 21 E. V. C. Yu. M. Koroteev, G. Bihlmayer and S. Bluegel, "First-principles investigation of structural and electronic properties of ultrathin Bi films," *Phys. Rev. B* **77**, 045428 (1–7) (2008).
- 22 S. McPhail, C. E. Yasin, A. R. Hamilton, M. Y. Simmons, E. H. Linfield, M. Pepper, and D. A. Ritchie, "Weak localization in high-quality two-dimensional systems," *Phys. Rev. B* **70**, 245311 (1–16) (2004).
- 23 M. Rudolph and J. J. Heremans, "Electronic and quantum phase coherence properties of bismuth thin films," *Appl. Phys. Lett.* **100**, 241601 (1–4) (2012).
- 24 B. Hackens, J. P. Minet, S. Faniel, G. Farhi, C. Gustin, J. P. Issi, J. P. Heremans, and V. Bayot, "Quantum transport, anomalous dephasing, and spin-orbit coupling in an open ballistic bismuth nanocavity," *Phys. Rev. B* **67**, 121403(R) (1–4) (2003).
- 25 J. C. Licini, G. J. Dolan, and D. J. Bishop, "Weakly localized behavior in quasi-one-dimensional Li films," *Phys. Rev. B* **54**, 1585–1588 (1985).
- 26 K. K. Choi, D. C. Tsui, and K. Alavi, "Dephasing time and one-dimensional localization of two-dimensional electrons in GaAs/AlGaAs heterostructures," *Phys. Rev. B* **36**, 7751–7754 (1987).
- 27 C. W. J. Beenakker and H. van Houten, "Boundary scattering and weak localization of electrons in a magnetic field," *Phys. Rev. B* **38**, 3232–3240 (1988).
- 28 G. J. Dolan, J. C. Licini, and D. J. Bishop, "Quantum interference in lithium ring arrays," *Phys. Rev. Lett.* **56**, 1493–1496 (1986).
- 29 A. Zduniak, M. Dyakonov, and W. Knap, "Universal behavior of magnetoconductance due to weak localization in two dimensions," *Phys. Rev. B* **56**, 1996–2003 (1997).
- 30 M. Ferrier, A. C. H. Rowe, S. Gueron, H. Bouchiat, C. Texier, and G. Montambaux, "Geometrical dependence of decoherence by electronic interactions in a GaAs/AlGaAs square network," *Phys. Rev. Lett.* **100**, 146802 (1–4) (2008).
- 31 B. Doucot and R. Rammal, "Interference effect and magnetoresistance oscillations in normal-metal networks: 1-weak localization approach," *J. Physique* **47**, 973–999 (1986).
- 32 R. Winkler, *Spin-orbit coupling effects in two-dimensional electron and hole systems*, Springer Tracts in Modern Physics 191, Springer-Verlag, Berlin Heidelberg (2003).
- 33 T. Koga, J. Nitta, T. Akazaki, and H. Takayanagi, "Rashba spin-orbit coupling probed by the weak antilocalization analysis in InAlAs/InGaAs/InAlAs quantum wells as a function of quantum well asymmetry," *Phys. Rev. Lett.* **89**, 046801 (1–4) (2002).
- 34 T. Fujita, M. B. A. Jalil, S. G. Tan, and S. Murakami, "Gauge fields in spintronics," *J. Appl. Phys.* **110**, 121301 (1–29) (2011).
- 35 W. Zawadzki, "Zitterbewegung and its effects on electrons in semiconductors," *Phys. Rev. B* **72**, 085217 (1–4) (2005).

## List of Figures

- 1 Magneto-resistance due to AL measured in Bi wires of widths 0.21, 0.33, 0.41 and 0.71  $\mu\text{m}$ .
- 2 Experimental values of  $L_{so}$  vs  $1/w$  for wires of width  $w$  fabricated on (a) an InSb 2D system, (b) an InAs 2D system, and (c) a Bi thin film.
- 3 Geometrical effects in wires of (a)  $w$ , and (b)  $L$ , on the AL signal  $\Delta R/R^2$ . In (a),  $w$  is varied (wide  $w$  at top, narrow  $w$  at bottom) and in (b)  $L$  is varied (long  $L$  at top, short  $L$  at bottom) as described in the text.